Special Issue

Imaging Foveal Microvasculature: Optical Coherence Tomography Angiography Versus Adaptive Optics Scanning Light Ophthalmoscope Fluorescein Angiography

Shelley Mo,[1,2] Brian Krawitz,[1,2] Eleni Efstathiadis,[2,3] Lawrence Geyman,[1,2] Rishard Weitz,[2] Toco Y. P. Chui,[1,2] Joseph Carroll,[4–6] Alfredo Dubra,[4–6] and Richard B. Rosen[1,2]

[1]Icahn School of Medicine at Mount Sinai, New York, New York, United States
[2]Ophthalmology, New York Eye and Ear Infirmary of Mount Sinai, New York, New York, United States
[3]William E. Macaulay Honors College, New York, New York, United States
[4]Ophthalmology, Medical College of Wisconsin, Milwaukee, Wisconsin, United States
[5]Biophysics, Medical College of Wisconsin, Milwaukee, Wisconsin, United States
[6]Cell Biology, Neurobiology & Anatomy, Medical College of Wisconsin, Milwaukee, Wisconsin, United States

Correspondence: Richard B. Rosen, 310 East 14th Street, 5th Floor South Building, New York, NY 10003, USA; rrosen@nyee.edu.

Submitted: December 14, 2015
Accepted: March 31, 2016

Citation: Mo S, Krawitz B, Efstathiadis E, et al. Imaging foveal microvasculature: optical coherence tomography angiography versus adaptive optics scanning light ophthalmoscope fluorescein angiography. *Invest Ophthalmol Vis Sci*. 2016;57:OCT130–OCT140. DOI:10.1167/iovs.15-18932

Purpose. To compare the use of optical coherence tomography angiography (OCTA) and adaptive optics scanning light ophthalmoscope fluorescein angiography (AOSLO FA) for characterizing the foveal microvasculature in healthy and vasculopathic eyes.

Methods. Four healthy controls and 11 vasculopathic patients (4 diabetic retinopathy, 4 retinal vein occlusion, and 3 sickle cell retinopathy) were imaged with OCTA and AOSLO FA. Foveal perfusion maps were semiautomatically skeletonized for quantitative analysis, which included foveal avascular zone (FAZ) metrics (area, perimeter, acircularity index) and vessel density in three concentric annular regions of interest. On each set of OCTA and AOSLO FA images, matching vessel segments were used for lumen diameter measurement. Qualitative image comparisons were performed by visual identification of microaneurysms, vessel loops, leakage, and vessel segments.

Results. Adaptive optics scanning light ophthalmoscope FA and OCTA showed no statistically significant differences in FAZ perimeter, acircularity index, and vessel densities. Foveal avascular zone area, however, showed a small but statistically significant difference of 1.8% ($P = 0.004$). Lumen diameter was significantly larger on OCTA (mean difference 5.7 μm, $P < 0.001$). Microaneurysms, fine structure of vessel loops, leakage, and some vessel segments were visible on AOSLO FA but not OCTA, while blood vessels obscured by leakage were visible only on OCTA.

Conclusions. Optical coherence tomography angiography is comparable to AOSLO FA at imaging the foveal microvasculature except for differences in FAZ area, lumen diameter, and some qualitative features. These results, together with its ease of use, short acquisition time, and avoidance of potentially phototoxic blue light, support OCTA as a tool for monitoring ocular pathology and detecting early disease.

Keywords: optical coherence tomography, angiography, retinal vasculature, adaptive optics, fluorescein angiography

The retina is one of the most metabolically active tissues in the human body,[1] requiring a complex vascular network to support its high energy demand.[2,3] Therefore, the retina is especially vulnerable to pathologic vascular changes. Alterations to capillary structure and perfusion have long been observed in retinal conditions such as diabetic retinopathy and are essential for diagnosing and monitoring disease.[4] Consequently, there is high demand for reliable in vivo visualization of the retinal microvasculature that is clinically accessible.

Intravenous fluorescein angiography (IV FA) remains the clinical gold standard for detecting vascular pathology in the retina since Novotny and Alvis[5] first demonstrated this technique in humans in 1961. However, it is an invasive test that requires exposure to an exogenous contrast agent. Though adverse effects of fluorescein are uncommon, they range from nausea and pruritus to anaphylaxis.[6] Moreover, the axial and lateral resolution of conventional IV FA, using traditional fundus cameras and scanning laser ophthalmoscopes, allow for limited visualization of capillaries, especially in areas of the retina in which there are overlapping capillary beds.[7]

With the ability to correct for the eye's monochromatic aberrations, adaptive optics (AO) offers improved resolution of retinal microvasculature over existing clinical imaging modalities. Adaptive optics scanning light ophthalmoscope fluorescein angiography (AOSLO FA) was first validated against histology in the primate retina[8] and has since been successfully demonstrated in human eyes, allowing for better resolution of the vasculature in comparison to conventional IV FA.[9] Recent AO studies have shown that oral fluorescein can be used in place of IV contrast with comparable results[9,10] and, because of slower gastrointes-

Investigative Ophthalmology & Visual Science

tinal absorption, it has the added advantage of accommodating the longer imaging times currently needed for AO. Though the side effects of oral fluorescein are milder,[11,12] anaphylaxis is still a possible consequence of administration.[13]

Optical coherence tomography angiography (OCTA) has recently emerged as a promising noninvasive way to visualize retinal microvasculature. Instead of exogenous contrast requiring blue light excitation, OCTA uses the motion of erythrocytes illuminated with near-infrared light to generate perfusion maps. The longer wavelength avoids the potential for photochemical damage, which could be especially important for diseased retinas.[14,15] Raw OCT data can be processed into OCTA images by using several different techniques including phase-based (e.g., phase variance OCT)[16,17] and amplitude-based (e.g., split-spectrum amplitude decorrelation angiography [SSADA])[18–21] methods. In comparing OCTA images from human subjects and confocal microscopic images from donor eyes, OCTA reveals the different retinal vascular layers as described in histology and with similar quantitative parameters such as FAZ area.[22,23] However, few studies have compared OCTA with other in vivo vascular imaging,[23–25] an important step in the validation of OCTA as a clinical tool to be used alongside familiar imaging modalities. Though AOSLO FA is not yet a routine clinical instrument, its ability to produce higher resolution images, compared to conventional IV FA, makes it an ideal modality to validate OCTA. In this study, we sought to evaluate OCTA in imaging the foveal microvasculature in comparison to AOSLO FA.

Methods

Subjects

This study adhered to the tenets of the Declaration of Helsinki and was approved by the Institutional Review Board at the New York Eye and Ear Infirmary of Mount Sinai. Four healthy controls and 11 patients with diabetic retinopathy (four subjects), retinal vein occlusion (four subjects), or sickle cell retinopathy (three subjects) were recruited. Inclusion criteria were as follows: clear natural lens, normal anterior segment, clear media, best corrected visual acuity better than 20/80, good fixation, and pupil dilation to at least 5 mm. Patients with severe macular edema were excluded owing to current limitations of AOSLO imaging and potentially excessive fluorescein leakage obscuring the microvasculature. Healthy controls were defined as having no prior retinal pathology or major systemic vascular disease. Patient diagnoses were determined from chart review and patient-reported history. Healthy controls were imaged with AOSLO FA and OCTA within 2 years (one subject was imaged on the same day; mean duration between imaging for the other three subjects was 13 months). All vasculopathic patients were imaged with AOSLO FA and OCTA on the same day. Written informed consent was obtained after discussion of the study methodology and risks and benefits. Best corrected visual acuity was assessed before any imaging or pupillary dilation. Pupils were dilated with one drop of 2.5% phenylephrine hydrochloride ophthalmic solution (Paragon BioTeck, Inc., Portland, OR, USA) and two drops of 1% tropicamide ophthalmic solution (Akorn, Inc., Lake Forest, IL, USA). Axial lengths were obtained with an IOL Master (Carl Zeiss Meditec, Inc., Dublin, CA, USA) to account for individual retinal magnification.

Adaptive Optics Scanning Light Ophthalmoscope Imaging and Image Processing

The AOSLO used in this study was a replica of the one described by Dubra and Sulai,[26] with modification of the visible channel to capture fluorescein signal. Briefly, three light sources with wavelengths of 488, 790, and 850 nm were used for fluorescein excitation, reflectance imaging, and wavefront sensing, respectively.[9] A 15-kHz horizontal resonant optical scanner and a 16-Hz vertical optical scanner were used to form a 1.75° square imaging raster. Light exposure was kept below maximum permissible exposure according to the American National Standards Institute ANSI Z136.[9,27]

For AOSLO FA, four vials of 10% fluorescein sodium (Akorn, Inc.), or approximately 20 mg/kg, were administered orally with orange juice or water depending on subject preference. Fifteen minutes after fluorescein administration, confocal reflectance and fluorescence sequences with optimal focus of the vascular layer on the fluorescein channel were acquired simultaneously with all three light sources. Subjects' gaze was directed with a green fixation target, which was moved as needed to image a $6 \times 6°$ ($\sim 1.8 \times 1.8$ mm) area centered at the fovea as previously described.[9] Adaptive optics scanning light ophthalmoscope FA image sequences, each with 125 frames, were collected at each retinal location. Additional confocal and nonconfocal (split detection) sequences of the same retinal regions were collected with optimal focus of the vascular layer on the split detection channel.[28] Subjects were encouraged to blink throughout the imaging session. Breaks were given approximately every 2 minutes or as needed. Total fluorescein imaging time was approximately 5 minutes, with an additional 5 minutes for confocal reflectance and split detection imaging.

To produce fluorescein images, fluorescence sequences were coregistered with corresponding confocal reflectance sequences as the primary sequence, and 5 to 100 frames with high signal-to-noise ratio from each of the original videos were averaged by using custom software.[29] These images were then manually montaged with Adobe Photoshop CS6 (Adobe Systems, Inc., San Jose, CA, USA). Nonconfocal split detection sequences were processed in the same manner.

Optical Coherence Tomography Angiography Imaging and Image Processing

Optical coherence tomography angiography imaging was performed by using the AngioVue system on the Optovue RTVue XR Avanti (Optovue, Inc., Fremont, CA, USA). This instrument is a spectral-domain OCT with a scan rate of 70,000 A-scans/s and a scan beam wavelength of 840 ± 10 nm (45-nm bandwidth). Macular $10 \times 10°$ ($\sim 3 \times 3$ mm) scans centered at the fovea were obtained for each subject. Each B-scan was composed of 304 A-scans. Two consecutive B-scans were obtained at each raster location for a total of 608 B-scans per volumetric raster scan, which amounted to an imaging time of 3 to 4 seconds per raster scan. Two raster scans (X-Fast and Y-Fast) were obtained. Perfusion maps were generated from the raw data by using the SSADA algorithm.[24,30,31]

With custom software, the en face superficial and deep perfusion maps generated by the AngioVue software were superimposed to create a single full microvasculature layer. Since AOSLO FA images the full microvascular layer, this superimposed OCTA image was used to compare the same vascular structures.

Quantitative Analysis of Microvasculature

Skeletonization, FAZ Metrics, and Vessel Density. To ensure that the regions quantified on corresponding images were the same, OCTA full layer images were registered with AOSLO FA images by using bUnwarpJ (Fig. 1).[32] The coregistered AOSLO FA and OCTA images were each semiautomatically skeletonized by using custom software on MATLAB (The MathWorks, Inc., Natick, MA, USA). Briefly, the

Investigative Ophthalmology & Visual Science

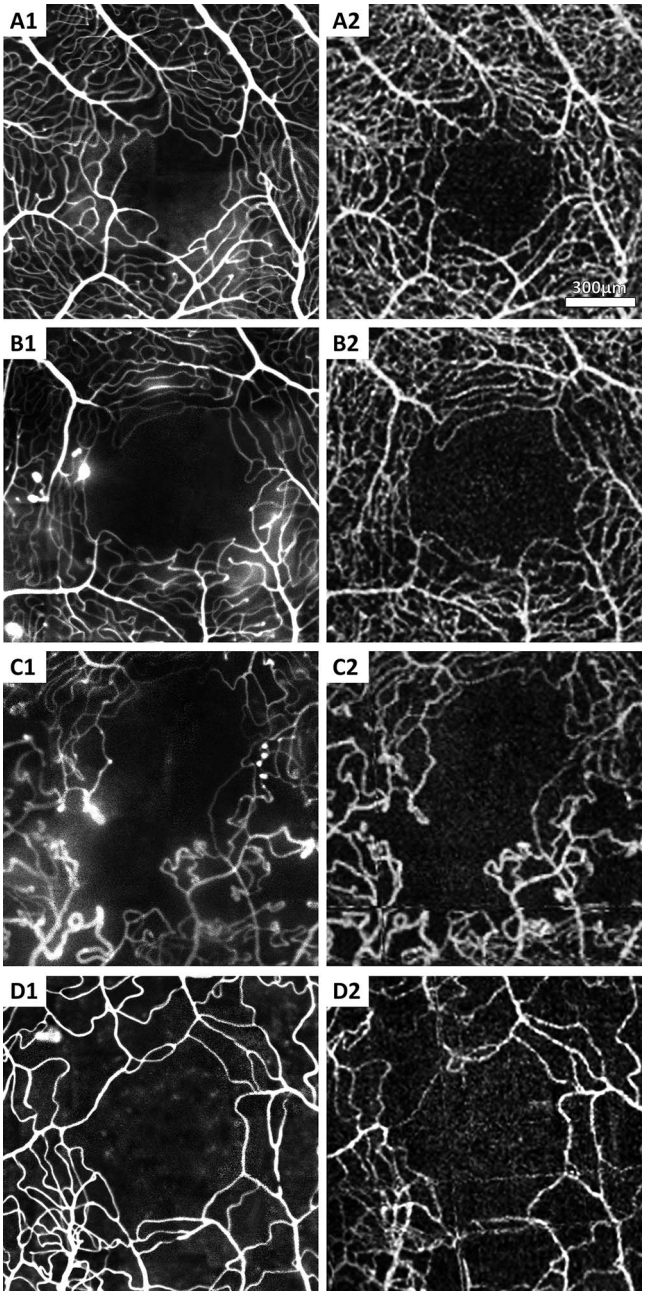

FIGURE 1. Adaptive optics scanning light ophthalmoscope FA (*left column*) and OCTA (*right column*) perfusion images centered at the fovea of four subjects. (**A**) Healthy control. (**B**) Diabetic retinopathy. (**C**) Retinal vein occlusion. (**D**) Sickle cell retinopathy.

software labels vessels as having a certain threshold pixel intensity and manual cleanup was done by an expert reader (SM). The skeleton data were used to calculate FAZ area, perimeter, and acircularity index (defined as the ratio of the perimeter of the FAZ and the perimeter of a circle with equal area),[33] as well as vessel density for each of the regions of interest (ROIs). Vessel density was defined as the total vessel length divided by the ROI area. The ROIs were defined as concentric rings with inner border at the FAZ margin and outer border at 100, 200, and 300 μm away from the FAZ margin (Fig. 2).[34,35] Intra- and interexaminer repeatability (second reader: BK) were performed on the FAZ metrics and vessel density at the 100-μm ROI in one randomly chosen set of images from each group.

Lumen Diameter. Lumen diameter was measured in 16 to 20 vessel segments in the AOSLO FA and OCTA images before registration with bUnwarpJ. These vessel segments of varying calibers and eccentricities were chosen to cover the broad spectrum of vascular structures seen on the scans (Fig. 3). Using custom software, a reader traces the center of the vessel of interest, ensuring that the sampled segment is at least 30 pixels long on OCTA (corresponding to approximately 40 μm) and 50 pixels long on AOSLO FA (corresponding to approximately 35 μm) (Hillard J, et al. *IOVS* 2013;54:ARVO E-Abstract 6061). The program straightens the segment and then samples the intensity of the pixels in a predefined ROI around the segment. An average cross-section of the intensities is generated, and the margins of the lumen are defined as the peak and trough in the derivative of the intensity profile. The minimum lengths of the segments were chosen in order to acquire enough pixel intensity data for a representative average curve.

Qualitative Comparisons of Microvasculature

Pathologic features noted during imaging were used to highlight the differences between AOSLO FA and OCTA. These included microaneurysms, vessel loops, leakage, and whether or not the vessel segment was identified with the skeletonization program. Differences in vessel identification were also mapped by using the 200-μm ROI skeletonizations. Adaptive optics scanning light ophthalmoscope FA and OCTA images were also compared to AOSLO confocal reflectance and split detection images to identify structural, as opposed to perfusion, differences among these imaging modalities.

Statistics

Statistical analysis was performed with Microsoft Excel (Microsoft Corporation, Redmond, WA, USA), SPSS 22.0 Statistical Software (IBM Corporation, Chicago, IL, USA), and R version 3.2.3.[36] For all statistical testing, $P < 0.05$ was considered significant. Before hypothesis testing, Anderson-Darling tests for normality were performed on each data set.[37] Sets of data in which normality could not be rejected when using the Anderson-Darling test were analyzed with paired *t*-tests. Sets of data found to be not normally distributed were analyzed with Wilcoxon signed rank tests. Bland-Altman plots[38] were created for each parameter. Intra- and interexaminer repeatability were assessed by using intraclass correlation coefficient (ICC). For the lumen diameter data, a linear mixed model was also generated to adjust for within-subject correlation among measurements and variation in number of measurements collected from each set of images.

RESULTS

Subject Characteristics

The mean ± SD age of the 15 subjects imaged was 40.7 ± 15.1 years. Six subjects were female (40%). See the Table for additional descriptors.

Foveal Avascular Zone Metric Agreement Between AOSLO FA and OCTA

Figure 4 (top row) shows the Bland-Altman plots of the FAZ area, perimeter, and acircularity index. The mean ± SD FAZ

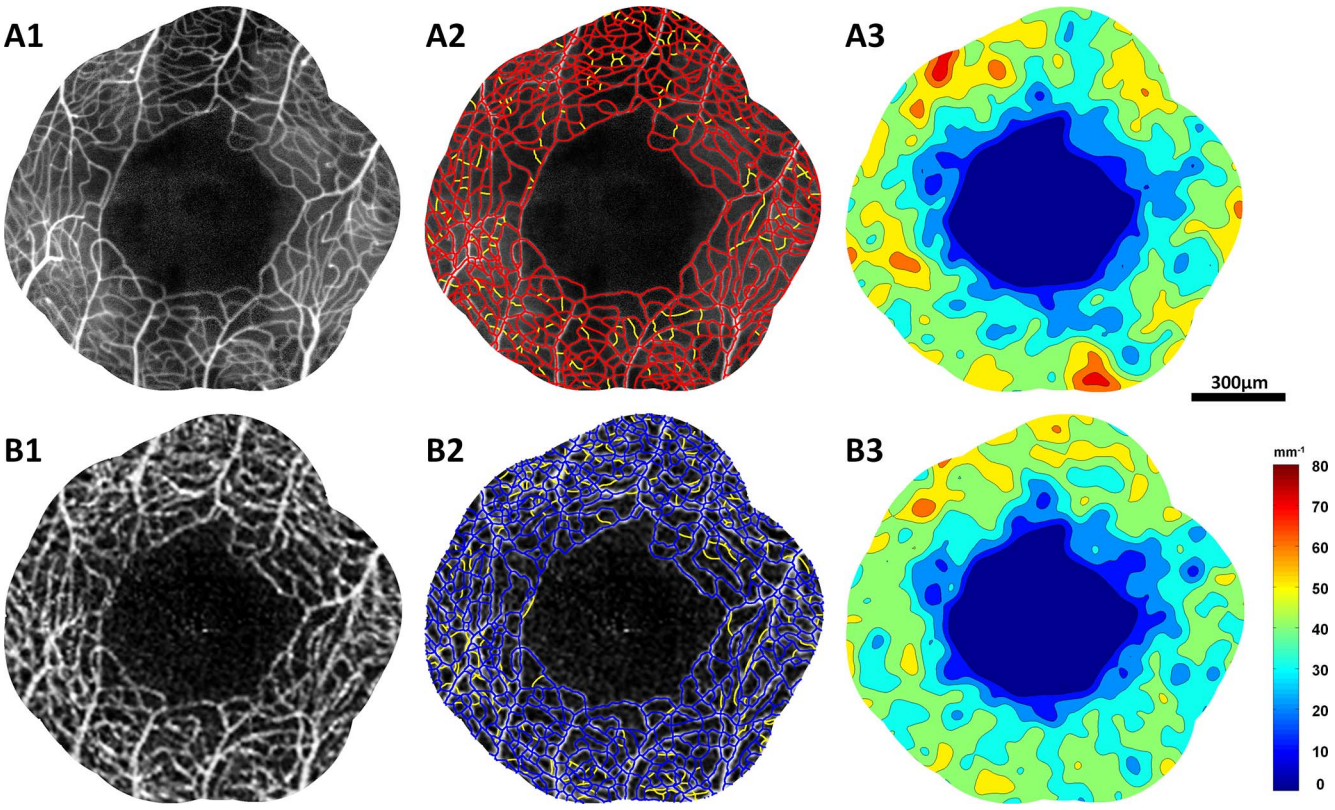

Figure 2. Adaptive optics scanning light ophthalmoscope FA (*top row*) and OCTA (*bottom row*) images of a healthy control subject (RR_0232). (**A1**, **B1**) Perfusion maps covering the 300-µm ROI. (**A2**, **B2**) Skeletonizations of perfusion maps with AOSLO FA in *red*, OCTA in *blue*; missing blood vessel segments seen on the other modality were indicated in *yellow*. (**A3**, **B3**) Density color contour maps produced from the skeletonizations.

area was 0.378 ± 0.245 mm^2 on AOSLO FA compared to 0.384 ± 0.249 mm^2 on OCTA. The mean ± SD percentage difference was 1.8% ± 1.2%, which was statistically significant (P = 0.004). The mean ± SD FAZ perimeter was 3.6 ± 1.9 mm on AOSLO FA compared to 3.5 ± 1.6 mm on OCTA. The mean ± SD percentage difference was 3.8% ± 4.1%, which was not statistically significant. The mean ± SD FAZ acircularity index was 1.67 ± 0.39 on AOSLO FA compared to 1.64 ± 0.30 on OCTA. The mean ± SD percentage difference from AOSLO FA to OCTA was 3.7% ± 4.1%, which was not statistically significant. All FAZ metrics showed high intra- and interexaminer repeatability (ICC > 0.9).

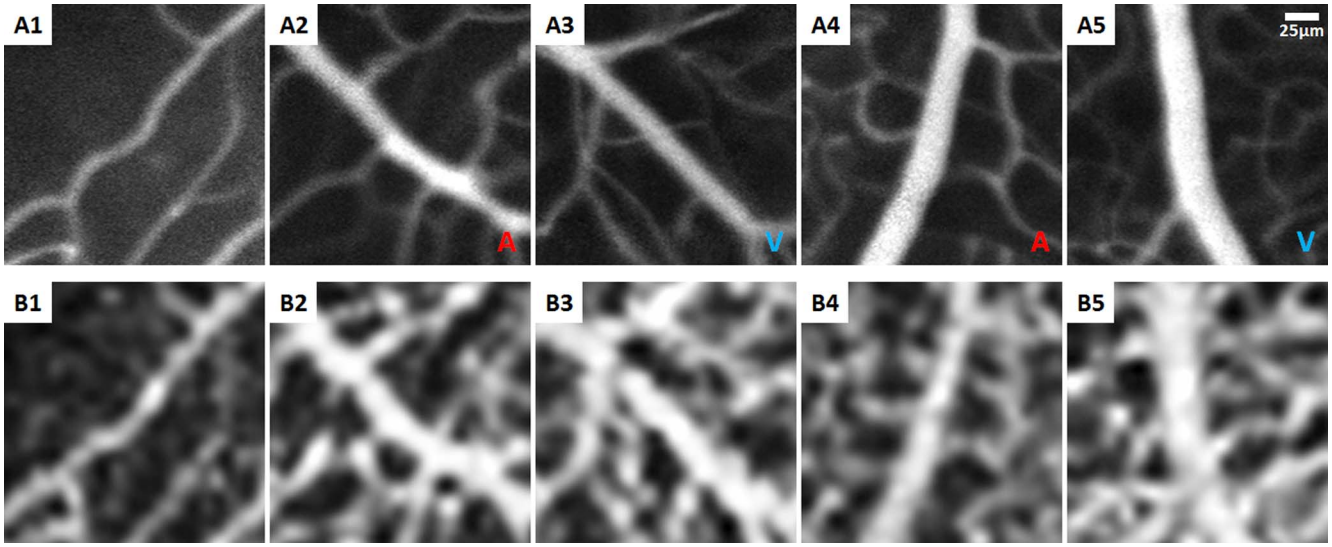

Figure 3. A selection of corresponding vessel segments with varying lumen diameters on AOSLO FA (*top row*) and OCTA (*bottom row*) images in a healthy control subject (RR_0424). (**A1**, **B1**) Capillary segment at the FAZ margin. (**A2–A5**, **B2–B5**) Arteriolar and venular segments located within 3° from the fovea. Arterial and venules are marked in A and V, respectively.

Investigative Ophthalmology & Visual Science

Table. Subject Characteristics

Subject ID	Age, y	Sex	Race	Eye Imaged
Healthy control				
RR_0113	22	F	Asian	OD
RR_0232	24	M	Asian	OD
RR_0424	25	M	Caucasian	OS
RR_0437	47	F	Caucasian	OD
Diabetic retinopathy				
RR_0205*	52	F	Asian	OD
RR_0217*	63	F	Caucasian	OS
RR_0366†	39	M	Hispanic	OD
RR_0449†	48	M	African American	OD
Retinal vein occlusion				
RR_0129	57	F	African American	OS
RR_0414	56	M	Hispanic/Caucasian	OD
RR_0443	45	M	Hispanic	OD
RR_0447	53	M	Asian	OS
Sickle cell retinopathy				
RR_0429	18	M	African American	OD
RR_0432	18	F	African American	OS
RR_0440	41	M	African American	OS

* Nonproliferative diabetic retinopathy.
† Proliferative diabetic retinopathy.

Vessel Density Agreement Between AOSLO FA and OCTA

Figure 4 (bottom row) shows the Bland-Altman plots of the vessel densities at each ROI. The mean ± SD densities on AOSLO FA at the 100-, 200-, and 300-µm ROI were 31.5 ± 4.2 mm^{-1}, 32.3 ± 6.0 mm^{-1}, and 34.4 ± 7.1 mm^{-1}, respectively, compared to 31.4 ± 4.3 mm^{-1}, 31.7 ± 6.0 mm^{-1}, and 33.6 ± 6.8 mm^{-1}, respectively, on OCTA. The mean ± SD percentage differences at each ROI were 4.2% ± 3.8%, 5.2% ± 5.6%, and 5.6% ± 4.8%, respectively. None of these differences were statistically significant. Vessel density at the 100-µm ROI showed high intra- and interexaminer repeatability (ICC > 0.9).

Larger Lumen Diameters on OCTA Than on AOSLO FA

A total of 273 vessel segments were measured for each modality (average of 17 per subject). The mean length of vessel segments measured was 102.2 µm on AOSLO FA and 102.6 µm on OCTA. The mean ± SD of lumen diameters measured on AOSLO FA was 14.2 ± 6.3 µm (3.6–38.7 µm) compared to 19.9 ± 5.9 µm (11–42 µm) on OCTA. The mean ± SD difference between OCTA and AOSLO FA measurements was 5.7 ± 3.2 µm. The Bland-Altman plot (Fig. 5) shows that OCTA measurements were generally larger and that there was no association between the mean lumen diameters and the raw differences. The linear mixed model yielded a highly significant coefficient of 5.7 for difference in modality ($P < 0.001$), supporting the mean difference from the Bland-Altman plot.

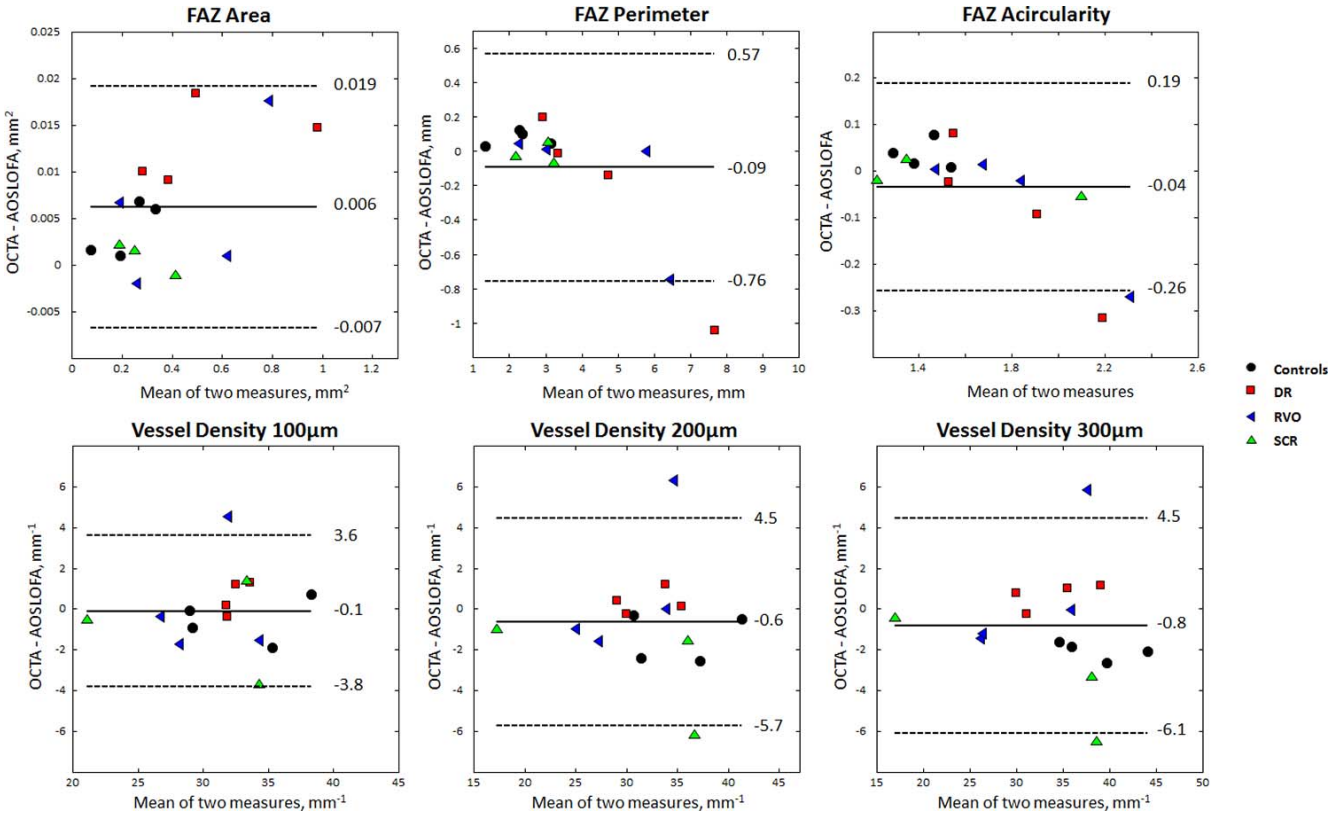

Figure 4. Bland-Altman plots showing differences between AOSLO FA and OCTA in FAZ metrics (*top row*) and vessel densities at each ROI (*bottom row*). Mean difference is shown by the *bold horizontal line* in each plot with 95% confidence interval shown by the *dashed horizontal lines*. Healthy controls are marked with *black circles*, diabetic retinopathy (DR) patients are marked with *red squares*, retinal vein occlusion (RVO) patients are marked with *blue triangles*, and sickle cell retinopathy (SCR) patients are marked with *green triangles*.

Investigative Ophthalmology & Visual Science

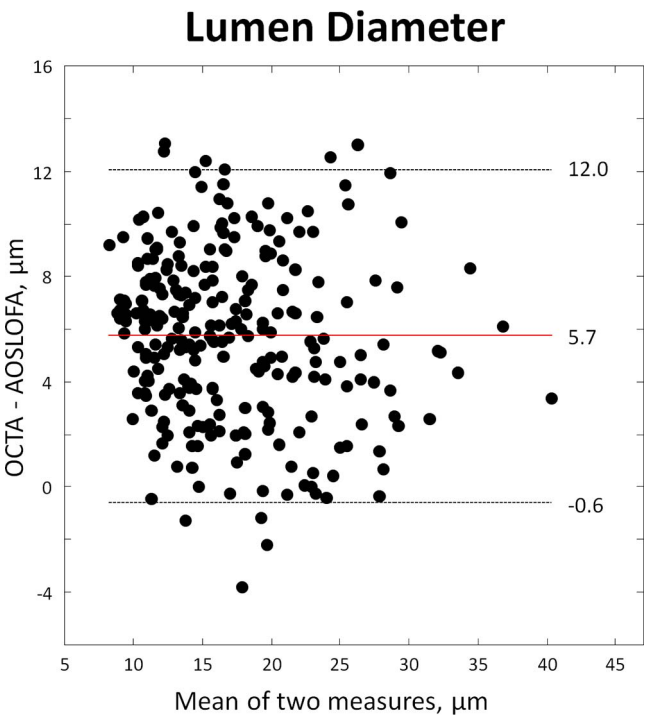

Figure 5. Bland-Altman plot showing differences between AOSLO FA and OCTA in lumen diameter measurements. Mean difference is shown by the *red horizontal line* with 95% confidence interval shown by the *dashed horizontal lines*.

Qualitative Comparisons of AOSLO FA and OCTA

Figure 6 shows representative images of the pathologic features noted on AOSLO FA versus OCTA. Microaneurysms were easily visible on AOSLO FA, but seen variably on OCTA. As shown in Figure 6B, vessels in the area of leakage were obscured on AOSLO FA, but no leakage was detected on OCTA as observed in previous studies[39,40] and therefore these vessels were visible. Vessel loops were present in both modalities but some of the finer structure was better captured on AOSLO FA. Some capillary segments were visualized on AOSLO FA but not on OCTA, likely owing to slow flow below the detection velocity threshold of 0.03 mm/s (Fig. 6D).

As shown in Figure 7, significant differences in vessel identification were observed between the two modalities. Notably, most of the vessel segments missing on AOSLO FA compared to OCTA were shorter than those missing on OCTA compared to AOSLO FA. Additionally, some of the latter differences were in vessels that appear to run very close to ones that were already identified on OCTA.

Figure 8 highlights the ability of AOSLO confocal reflectance and split detection imaging to capture nonperfused vessels that were neither visible on AOSLO FA nor OCTA in a subject with proliferative diabetic retinopathy (RR_0449). On the confocal image, these nonperfused vessels appeared less evenly reflective, while on the split detection image, they appeared flatter and had thinner walls.

Discussion

In this study, we examined the similarities and differences between AOSLO FA and OCTA, finding good agreement in FAZ metrics and vessel density. Lumen diameter was, however, generally larger on OCTA than on AOSLO FA, likely owing to lower sampling and image resolution (diffraction) and/or low-pass filtering within or after the SSADA algorithm in the former. Qualitative differences included visibility of microaneurysms, fine structure of vessel loops, leakage, and some capillary segments. These differences may be due to limitations in OCTA such as its detection velocity threshold and resolution.

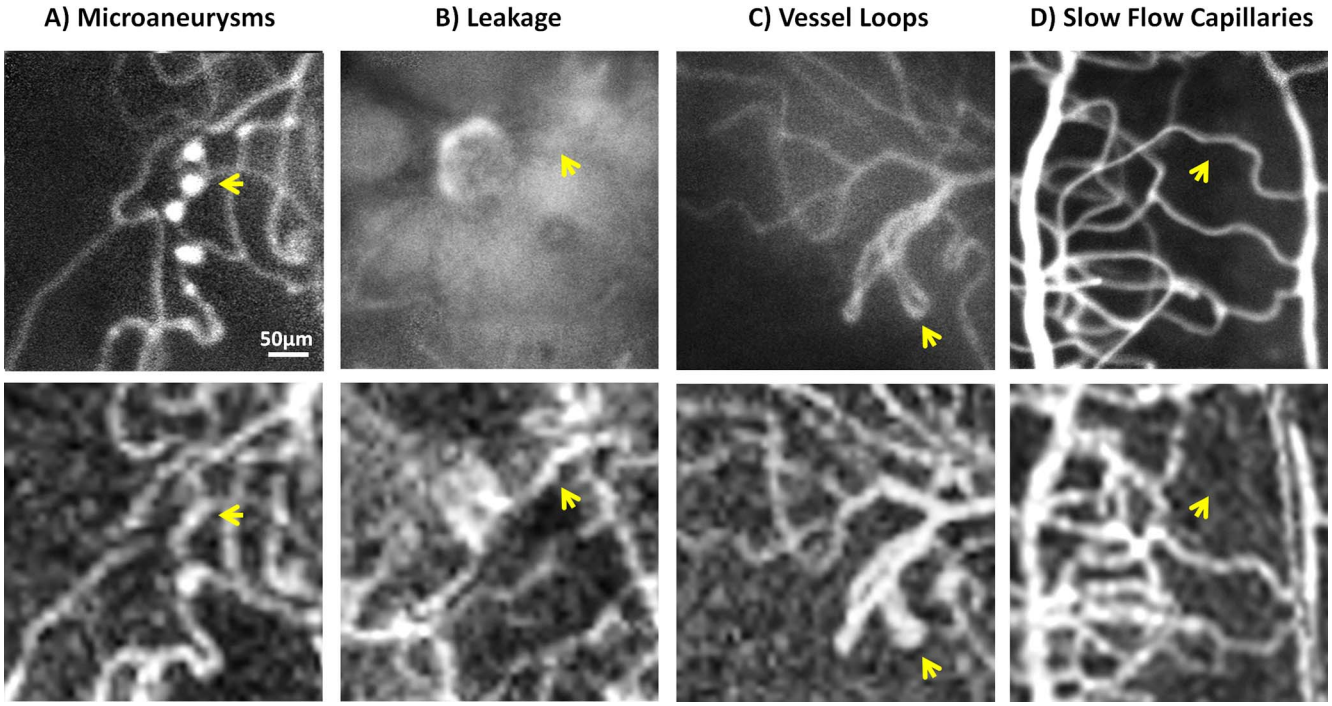

Figure 6. Representative images of pathologic features seen with AOSLO FA (*top row*) and OCTA (*bottom row*); *yellow arrows* highlight differences. (**A**) Microaneurysms seen on AOSLO FA but not OCTA. (**B**) Leakage obscuring a vessel on AOSLO FA, but the same vessel is visible on OCTA. (**C**) Vessel loop fine structure was seen clearly on AOSLO FA but is not as well delineated on OCTA. (**D**) Capillaries with slow flow seen on AOSLO FA but not on OCTA.

Investigative Ophthalmology & Visual Science

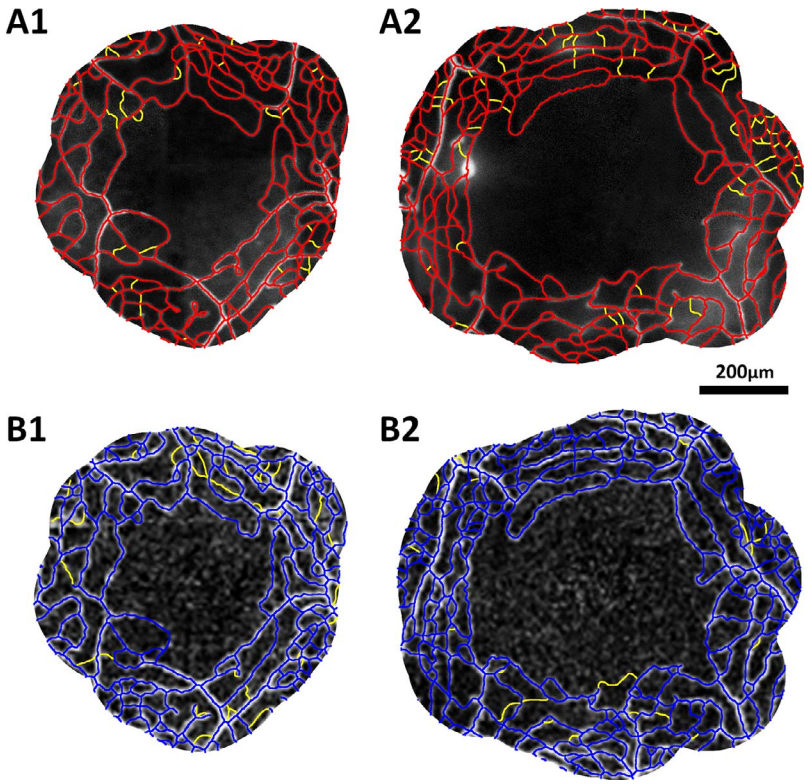

Figure 7. Skeletonizations of AOSLO FA (*top row*, *red*) and OCTA (*bottom row*, *blue*) images covering the 200-µm ROI in (1) a healthy control subject (RR_0424) and (2) a diabetic retinopathy subject (RR_0217). Missing vessel segments compared to the other modality are highlighted in *yellow*.

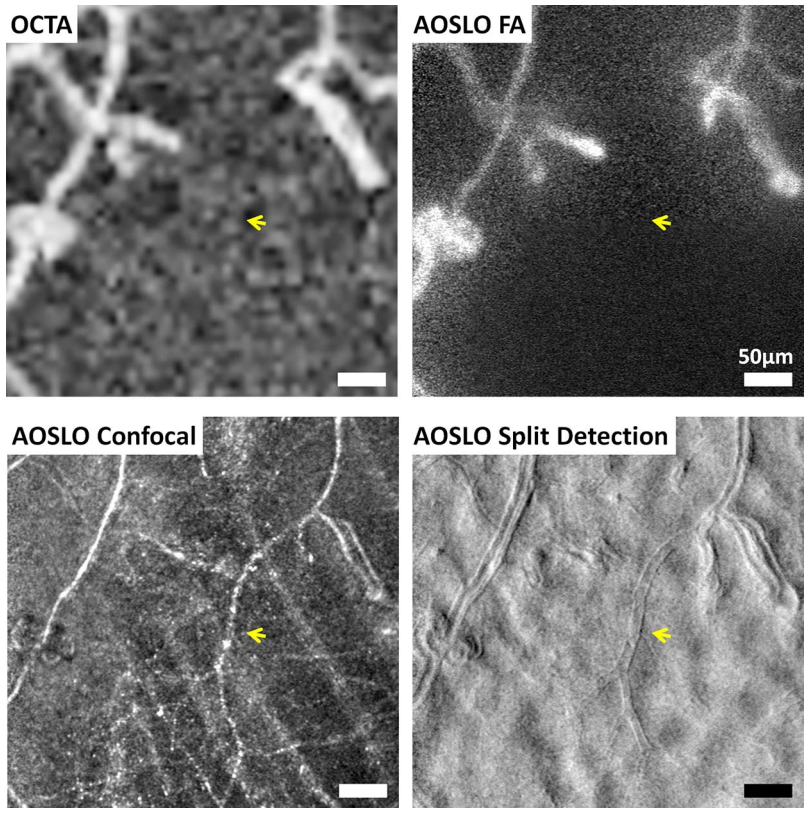

Figure 8. Imaging nonperfused capillaries in a subject with diabetic retinopathy (RR_0449) using AOSLO. Nonperfused capillaries (*yellow arrows*) are clearly visible on AOSLO confocal reflectance and AOSLO split detection (*bottom row*) but not on OCTA and AOSLO FA (*top row*).

Investigative Ophthalmology & Visual Science

The major limitations of this study were as follows: (1) the sample was small and nonrandom secondary to strict AOSLO selection criteria, particularly regarding patients with severe macular edema or medial opacities; (2) the AOSLO image processing and analysis using skeletonization are tedious and not clinically accessible; and (3) the area imaged was limited to the perifovea.

Capillary dropout is a prominent feature of vasoocclusive retinal diseases. Changes in the FAZ have been shown to be a good indicator of capillary dropout and are associated with disease progression. In particular, enlargement of the FAZ seems to be correlated with reduced visual acuity.[41,42] Therefore, the ability to track changes in FAZ structure is important for monitoring the progression and treatment of these diseases. The area, perimeter, and acircularity reported here are consistent with previous studies on healthy and diseased eyes.[25,34,35,41,43–52] The small but statistically significant difference of 1.8% in area could be explained by differences in detection of capillary segments that make up the FAZ margin, especially in vasculopathic eyes. This finding is likely due to blood flow that is slower than the detection velocity threshold of 0.3 mm/s on OCTA[53] or intermittent flow through these capillaries. Diabetic and sickle cell patients have been shown to have slower blood flow velocity in perifoveal capillaries as compared to healthy individuals.[42,44,50,54–56] Similar observations have been made in the vascular distributions affected by retinal vein occlusion.[57] Flower et al.[58] have shown that red blood cells move at varying velocities and even pause intermittently as they travel through retinal capillaries. It may be that during the few seconds required to obtain the scans for OCTA, the flow in some capillary segments is paused, resulting in nondetection of those segments (Supplementary Video S1, courtesy of Drew Scoles). Additionally, registration of the OCTA images to the AOSLO FA images should have removed most of the differences due to scaling and distortion from the optics of each instrument; however, we cannot rule out a small contribution from these factors (Supplementary Fig. S1). The small difference in FAZ area taken together with the statistically insignificant differences in perimeter and acircularity suggest that OCTA and AOSLO FA are comparable in their abilities to visualize and quantify FAZ structure.

Vessel density, in addition to FAZ structure, can be useful in quantifying capillary dropout. The density results in the present study are consistent with data from previous publications.[33,35] We found that vessel density was not significantly different between the two imaging modalities, though there was a trend toward increasingly lower densities in OCTA than in AOSLO FA as the ROI expanded farther away from the foveal center. Since the vascular networks become more complex with multiple overlapping capillary beds away from the foveal center, enface OCTA images may not be able to display some of the finer capillary structure, resulting in this trend toward lower densities. Another source of this difference may be our use of 2D projections of 3D OCT data in order to make the full microvascular layer comparison with AOSLO FA, perhaps resulting in some loss of angiographic data. However, our current study examined retinal regions in which the vasculature is organized into one or two layers, especially in the 100- and 200-μm ROI, so this projection issue should not have greatly influenced the density data. Future studies should analyze the layers captured on OCTA separately to generate more accurate data in regions of the retina where there are multiple overlapping capillary beds. Adaptive optics scanning light ophthalmoscope FA has also been shown to be limited in regions with multiple capillary layers, since it cannot simultaneously bring superficial and deeper capillaries into focus.[59] Adaptive optics scanning light ophthalmoscopy should ideally be performed by taking multiple videos of the same retinal region at different foci in order to thoroughly image the full retinal thickness. However, since FA imaging requires exposure of the retina to blue light, this repeated imaging at each retinal area of interest cannot be safely done with AOSLO FA. Thus, agreement between OCTA and AOSLO FA may only apply in areas of the retina where the vasculature is relatively simple and has few layers, such as at the fovea.

We observed that there are a number of vessel segments missing on OCTA compared to AOSLO FA. There are several sources for this difference. First, AOSLO FA has higher spatial sampling and lateral resolution than OCTA. Fine structures such as two closely adjacent capillaries or vessel loops seen on AOSLO FA may appear on OCTA to be a single vessel or a microaneurysm, respectively. Thus, OCTA is not an ideal tool to monitor changes in these fine structures. Second, similar to the reasoning behind the difference in FAZ area, some of the capillaries may have intermittent flow or slower blood flow velocity, especially in vasculopathic eyes. This observation raises an interesting clinical application; in combination with exogenous contrast-enhanced imaging such as IV FA, OCTA has the potential to identify vessels at risk for complete occlusion, since they will appear faint or absent on OCTA but apparent with exogenous contrast.

Compared to AOSLO FA, OCTA is more prone to eye motion artifacts and has lower lateral resolution, resulting in the differences in lumen diameter and appearance of vessels between the two modalities. Since the sources of the perfusion signal (i.e., fluorescein for AOSLO FA and red blood cells for OCTA) are confined to the intraluminal space, the images produced should represent the vessel lumen. Lumen diameters of retinal capillaries near the FAZ in histologic and previous AO studies are approximately 5 to 10 μm,[60,61] which is in agreement with the present AOSLO FA data. Yet, as this and previous studies have shown, vessels on OCTA look more heterogeneous, do not have a smooth appearance, and have larger diameter than on histology or AOSLO.[22,62–64] This lumen diameter discrepancy is likely due to the lower lateral resolution on OCTA. It has been proposed that perhaps the heterogeneous, beaded appearance of vessels on OCTA may be due to pulsatile flow, local pericyte constriction, and/or nonuniform distribution of erythrocytes and leukocytes in capillaries.[22,62,63] Eye movement within and between B-scans likely contribute to the uneven appearance as well. One way to correct for this artifactual uneven appearance and varying intensity along a vessel segment may be to average multiple registered OCTA scans, as illustrated in Figure 9. Further work is needed to quantify the quality of these averaged images and to evaluate the potential for this technique to improve OCTA.

In agreement with previous studies,[39,40] we found differences in the visualization of leakage and microaneurysms on OCTA compared to AOSLO FA. Leakage has been shown to be important in the diagnosis, monitoring, and treatment of a number of retinal diseases, including diabetic retinopathy and retinal vascular occlusions; microaneurysm formation also contributes to the diagnosis of retinal vasculopathy, and detection of leaking microaneurysms on IV FA can direct localized treatment such as laser photocoagulation for macular edema.[65–73] Since OCTA is unable to consistently show these pathologic features, owing to slow or intermittent blood flow, it may be useful to pair it with another modality such as fundus photography or IV FA for more complete clinical assessment. Vascular changes in which there is adequate flow velocity are easily visible with OCTA and can be localized axially.[39] For example, Figure 10 shows that the dilated vessels in two branch retinal vein occlusion patients are located primarily in the deep plexus. This ability to axially locate pathologic vascular changes may help further our understanding of the natural history of retinal diseases.

Investigative Ophthalmology & Visual Science

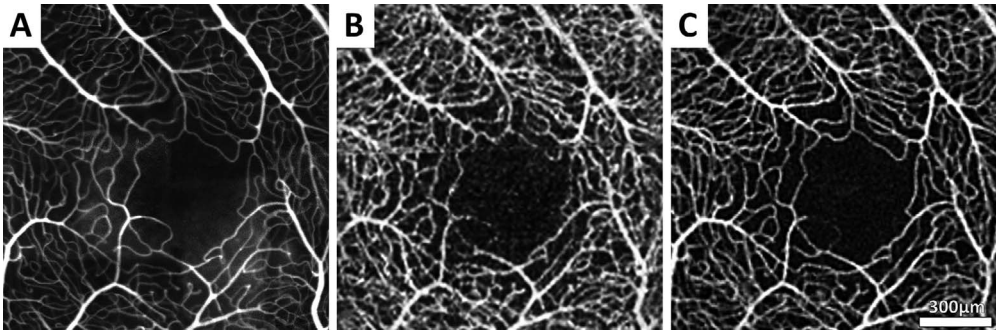

Figure 9. Images from a healthy control subject (RR_0424). (**A**) Adaptive optics scanning light ophthalmoscope FA perfusion map. (**B**) Optical coherence tomography angiography full vessel layer perfusion map generated from a single scan with AngioVue software. (**C**) Optical coherence tomography angiography full vessel layer generated from registering and averaging five scans with custom MATLAB software.[74]

Conclusions

Optical coherence tomography angiography foveal microvascular images appear comparable to AOSLO FA. With its ease of use, noninvasive nature, and short scan time, OCTA is an attractive option for retinal disease screening. In addition, OCTA uniquely delineates multiple capillary layers in a single volumetric scan and is able to reveal blood vessels obscured by leakage. In its current form, however, low scanning speed and resolution limit its ability to visualize important pathologic features such as microaneurysms, leakage, and vessel loops. Technologic improvements, such as eye motion compensation, could lead to its broad adoption as a noninvasive method for detecting retinal vascular disease.

Acknowledgments

The authors would like to thank Patricia Garcia, Nadim Choudhury, and Nikhil Menon for their assistance in collecting some of the images used in this study and Drew Scoles for the supplementary video.

Supported by National Eye Institute of the National Institutes of Health under Award No. P30EY001931 and U01EY025477. The content is solely the responsibility of the authors and does not necessarily represent the official views of the National Institutes of Health. Funding for this research was provided by the Marrus Family Foundation, Bendheim-Lowenstein Family Foundation, Wise Family Foundation, New York Eye and Ear Chairman's Research Fund, Violett Fund, Milbank Foundation, and Glaucoma Research Foundation Catalyst for a Cure Initiative. The sponsors and funding organizations had no role in the design or conduct of this research.

Disclosure: **S. Mo**, None; **B. Krawitz**, None; **E. Efstathiadis**, None; **L. Geyman**, None; **R. Weitz**, Notal Vision (C), Nano Retina (C); **T.Y.P. Chui**, None; **J. Carroll**, Optovue (F); **A. Dubra**, P; **R.B. Rosen**, Genentech (F), Opticology (I), Nano Retina (C), Clarity (C), OD-OS (C), Allergan (C), Carl Zeiss Meditec (C), Optovue (C), Advanced Cellular Technologies (C), Regeneron (C),

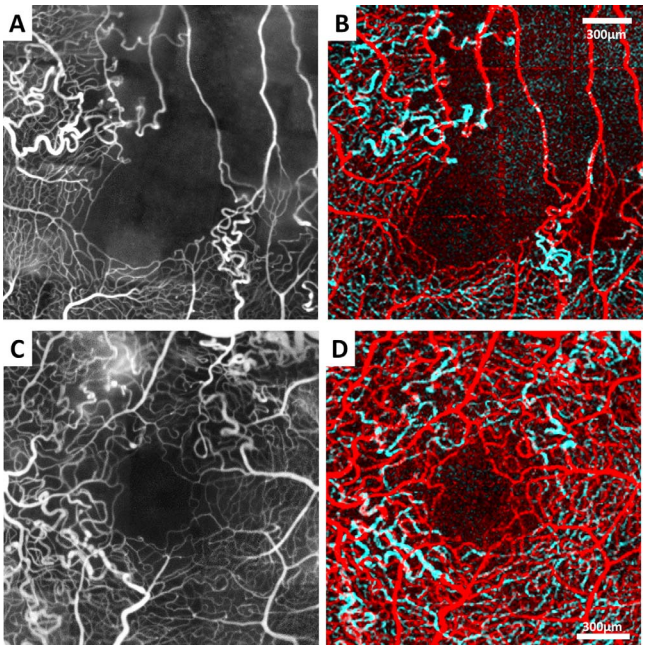

Figure 10. Visualization of the superficial and deep capillary plexus. Images from two subjects with retinal vein occlusion (*top row*: RR_0129; *bottom row*: RR_0414). (**A**, **C**) Adaptive optics scanning light ophthalmoscope FA. (**B**, **D**) Optical coherence tomography angiography color overlay with superficial vessels in *red* and deeper vessels in *cyan*.

References

1. Adler FH. Further notes on the metabolism of the retina. *Trans Am Ophthalmol Soc*. 1931;29:233–241.
2. Snodderly DM, Weinhaus RS, Choi JC. Neural-vascular relationships in central retina of macaque monkeys (Macaca fascicularis). *J Neurosci*. 1992;12:1169–1193.
3. Yu PK, Balaratnasingam C, Cringle SJ, McAllister IL, Provis J, Yu DY. Microstructure and network organization of the microvasculature in the human macula. *Invest Ophthalmol Vis Sci*. 2010;51:6735–6743.
4. Bek T. Regional morphology and pathophysiology of retinal vascular disease. *Prog Retin Eye Res*. 2013;36:247–259.
5. Novotny HR, Alvis DL. A method of photographing fluorescence in circulating blood in the human retina. *Circulation*. 1961;24:82–86.
6. Yannuzzi LA, Rohrer KT, Tindel LJ, et al. Fluorescein angiography complication survey. *Ophthalmology*. 1986;93:611–617.
7. Mendis KR, Balaratnasingam C, Yu P, et al. Correlation of histologic and clinical images to determine the diagnostic value of fluorescein angiography for studying retinal capillary detail. *Invest Ophthalmol Vis Sci*. 2010;51:5864–5869.
8. Scoles D, Gray DC, Hunter JJ, et al. In-vivo imaging of retinal nerve fiber layer vasculature: imaging histology comparison. *BMC Ophthalmol*. 2009;9:9.
9. Pinhas A, Dubow M, Shah N, et al. In vivo imaging of human retinal microvasculature using adaptive optics scanning light ophthalmoscope fluorescein angiography. *Biomed Opt Express*. 2013;4:1305–1317.

10. Dubow M, Pinhas A, Shah N, et al. Classification of human retinal microaneurysms using adaptive optics scanning light ophthalmoscope fluorescein angiography. *Invest Ophthalmol Vis Sci*. 2014;55:1299–1309.
11. Hara T, Inami M. Efficacy and safety of fluorescein angiography with orally administered sodium fluorescein. *Am J Ophthalmol*. 1998;126:560–564.
12. Watson AP, Rosen ES. Oral fluorescein angiography: reassessment of its relative safety and evaluation of optimum conditions with use of capsules. *Br J Ophthalmol*. 1990;74:458–461.
13. Gomez-Ulla F, Gutierrez C, Seoane I. Severe anaphylactic reaction to orally administered fluorescein. *Am J Ophthalmol*. 1991;112:94.
14. Paskowitz DM, LaVail MM, Duncan JL. Light and inherited retinal degeneration. *Br J Ophthalmol*. 2006;90:1060–1066.
15. Cideciyan AV, Jacobson SG, Aleman TS, et al. In vivo dynamics of retinal injury and repair in the rhodopsin mutant dog model of human retinitis pigmentosa. *Proc Natl Acad Sci U S A*. 2005;102:5233–5238.
16. Kim DY, Fingler J, Werner JS, Schwartz DM, Fraser SE, Zawadzki RJ. In vivo volumetric imaging of human retinal circulation with phase-variance optical coherence tomography. *Biomed Opt Express*. 2011;2:1504–1513.
17. Fingler J, Zawadzki RJ, Werner JS, Schwartz D, Fraser SE. Volumetric microvascular imaging of human retina using optical coherence tomography with a novel motion contrast technique. *Opt Express*. 2009;17:22190–22200.
18. Enfield J, Jonathan E, Leahy M. In vivo imaging of the microcirculation of the volar forearm using correlation mapping optical coherence tomography (cmOCT). *Biomed Opt Express*. 2011;2:1184–1193.
19. Jia Y, Tan O, Tokayer J, et al. Split-spectrum amplitude-decorrelation angiography with optical coherence tomography. *Opt Express*. 2012;20:4710–4725.
20. Mariampillai A, Standish BA, Moriyama EH, et al. Speckle variance detection of microvasculature using swept-source optical coherence tomography. *Opt Lett*. 2008;33:1530–1532.
21. Motaghiannezam R, Fraser S. Logarithmic intensity and speckle-based motion contrast methods for human retinal vasculature visualization using swept source optical coherence tomography. *Biomed Opt Express*. 2012;3:503–521.
22. Tan PE, Balaratnasingam C, Xu J, et al. Quantitative comparison of retinal capillary images derived by speckle variance optical coherence tomography with histology. *Invest Ophthalmol Vis Sci*. 2015;56:3989–3996.
23. Mammo Z, Balaratnasingam C, Yu P, et al. Quantitative noninvasive angiography of the fovea centralis using speckle variance optical coherence tomography. *Invest Ophthalmol Vis Sci*. 2015;56:5074–5086.
24. Spaide RF, Klancnik JM Jr, Cooney MJ. Retinal vascular layers imaged by fluorescein angiography and optical coherence tomography angiography. *JAMA Ophthalmol*. 2015;133:45–50.
25. Kim DY, Fingler J, Zawadzki RJ, et al. Noninvasive imaging of the foveal avascular zone with high-speed, phase-variance optical coherence tomography. *Invest Ophthalmol Vis Sci*. 2012;53:85–92.
26. Dubra A, Sulai Y. Reflective afocal broadband adaptive optics scanning ophthalmoscope. *Biomed Opt Express*. 2011;2:1757–1768.
27. Delori FC, Webb RH, Sliney DH. Maximum permissible exposures for ocular safety (ANSI 2000), with emphasis on ophthalmic devices. *J Opt Soc Am A Opt Image Sci Vis*. 2007;24:1250–1265.
28. Sulai YN, Scoles D, Harvey Z, Dubra A. Visualization of retinal vascular structure and perfusion with a nonconfocal adaptive optics scanning light ophthalmoscope. *J Opt Soc Am A Opt Image Sci Vis*. 2014;31:569–579.
29. Dubra A, Harvey Z. Registration of 2D images from fast scanning ophthalmic instruments. *The 4th International Workshop on Biomedical Image Registration*. Lübeck, Germany; 2010.
30. Spaide RF, Klancnik JM Jr, Cooney MJ. Retinal vascular layers in macular telangiectasia type 2 imaged by optical coherence tomographic angiography. *JAMA Ophthalmol*. 2015;133:66–73.
31. Agemy SA, Scripsema NK, Shah CM, et al. Retinal vascular perfusion density mapping using optical coherence tomography angiography in normals and diabetic retinopathy patients. *Retina*. 2015;35:2353–2363.
32. Arganda-Carreras I, Sorzano CS, Marabini R, Carazo J, Ortiz-de-Solorzano C, Kybic J. Consistent and elastic registration of histological sections using vector-spline regularization. In: Beichel R, Sonka M, eds. *Computer Vision Approaches to Medical Image Analysis*. Berlin, Heidelberg: Springer Berlin Heidelberg; 2006:85–95.
33. Tam J, Dhamdhere KP, Tiruveedhula P, et al. Disruption of the retinal parafoveal capillary network in type 2 diabetes before the onset of diabetic retinopathy. *Invest Ophthalmol Vis Sci*. 2011;52:9257–9266.
34. Tam J, Dhamdhere KP, Tiruveedhula P, et al. Subclinical capillary changes in non-proliferative diabetic retinopathy. *Optom Vis Sci*. 2012;89:E692–E703.
35. Tam J, Martin JA, Roorda A. Noninvasive visualization and analysis of parafoveal capillaries in humans. *Invest Ophthalmol Vis Sci*. 2010;51:1691–1698.
36. R Core Team. *R: A Language and Environment for Statistical Computing*. Vienna, Austria: R Foundation for Statistical Computing; 2015.
37. Anderson TW, Darling DA. Asymptotic theory of certain "goodness-of-fit" criteria based on stochastic processes. *Ann Math Stat*. 1952;23:193–212.
38. Altman DG, Bland JM. Measurement in medicine—the analysis of method comparison studies. *Statistician*. 1983;32:307–317.
39. Jia Y, Bailey ST, Hwang TS, et al. Quantitative optical coherence tomography angiography of vascular abnormalities in the living human eye. *Proc Natl Acad Sci U S A*. 2015;112:E2395–E2402.
40. Hwang TS, Jia Y, Gao SS, et al. Optical coherence tomography angiography features of diabetic retinopathy. *Retina*. 2015;35:2371–2376.
41. Parodi MB, Visintin F, Della Rupe P, Ravalico G. Foveal avascular zone in macular branch retinal vein occlusion. *Int Ophthalmol*. 1995;19:25–28.
42. Arend O, Wolf S, Harris A, Reim M. The relationship of macular microcirculation to visual acuity in diabetic patients. *Arch Ophthalmol*. 1995;113:610–614.
43. Bresnick GH, Condit R, Syrjala S, Palta M, Groo A, Korth K. Abnormalities of the foveal avascular zone in diabetic retinopathy. *Arch Ophthalmol*. 1984;102:1286–1293.
44. Arend O, Wolf S, Jung F, et al. Retinal microcirculation in patients with diabetes mellitus: dynamic and morphological analysis of perifoveal capillary network. *Br J Ophthalmol*. 1991;75:514–518.
45. John D, Kuriakose T, Devasahayam S, Braganza A. Dimensions of the foveal avascular zone using the Heidelberg retinal angiogram-2 in normal eyes. *Indian J Ophthalmol*. 2011;59:9–11.
46. Laatikainen L, Larinkari J. Capillary-free area of the fovea with advancing age. *Invest Ophthalmol Vis Sci*. 1977;16:1154–1157.
47. Takase N, Nozaki M, Kato A, Ozeki H, Yoshida M, Ogura Y. Enlargement of foveal avascular zone in diabetic eyes evaluated by en face optical coherence tomography angiography. *Retina*. 2015;35:2377–2383.

Investigative Ophthalmology & Visual Science

48. Conrath J, Giorgi R, Raccah D, Ridings B. Foveal avascular zone in diabetic retinopathy: quantitative vs qualitative assessment. *Eye (Lond)*. 2005;19:322–326.
49. Di G, Weihong Y, Xiao Z, et al. A morphological study of the foveal avascular zone in patients with diabetes mellitus using optical coherence tomography angiography. *Graefes Arch Clin Exp Ophthalmol*. 2016;254:873–879.
50. Wolf S, Arend O, Toonen H, Bertram B, Jung F, Reim M. Retinal capillary blood flow measurement with a scanning laser ophthalmoscope: preliminary results. *Ophthalmology*. 1991; 98:996–1000.
51. Chui TY, VanNasdale DA, Elsner AE, Burns SA. The association between the foveal avascular zone and retinal thickness. *Invest Ophthalmol Vis Sci*. 2014;55:6870–6877.
52. Dubis AM, Hansen BR, Cooper RF, Beringer J, Dubra A, Carroll J. Relationship between the foveal avascular zone and foveal pit morphology. *Invest Ophthalmol Vis Sci*. 2012;53:1628–1636.
53. Tokayer J, Jia Y, Dhalla AH, Huang D. Blood flow velocity quantification using split-spectrum amplitude-decorrelation angiography with optical coherence tomography. *Biomed Opt Express*. 2013;4:1909–1924.
54. Roy MS, Gascon P, Giuliani D. Macular blood flow velocity in sickle cell disease: relation to red cell density. *Br J Ophthalmol*. 1995;79:742–745.
55. Goldberg MF. Retinal vaso-occlusion in sickling hemoglobinopathies. *Birth Defects Orig Artic Ser*. 1976;12:475–515.
56. Stevens TS, Busse B, Lee CB, Woolf MB, Galinos SO, Goldberg MF. Sickling hemoglobinopathies: macular and perimacular vascular abnormalities. *Arch Ophthalmol*. 1974;92:455–463.
57. Avila CP Jr, Bartsch DU, Bitner DG, et al. Retinal blood flow measurements in branch retinal vein occlusion using scanning laser Doppler flowmetry. *Am J Ophthalmol*. 1998;126:683–690.
58. Flower R, Peiretti E, Magnani M, et al. Observation of erythrocyte dynamics in the retinal capillaries and choriocapillaris using ICG-loaded erythrocyte ghost cells. *Invest Ophthalmol Vis Sci*. 2008;49:5510–5516.
59. Pinhas A, Razeen M, Dubow M, et al. Assessment of perfused foveal microvascular density and identification of nonperfused capillaries in healthy and vasculopathic eyes. *Invest Ophthalmol Vis Sci*. 2014;55:8056–8066.
60. Rha J, Jonnal RS, Thorn KE, Qu J, Zhang Y, Miller DT. Adaptive optics flood-illumination camera for high speed retinal imaging. *Opt Express*. 2006;14:4552–4569.
61. Weinhaus RS, Burke JM, Delori FC, Snodderly DM. Comparison of fluorescein angiography with microvascular anatomy of macaque retinas. *Exp Eye Res*. 1995;61:1–16.
62. Chan G, Balaratnasingam C, Xu J, et al. In vivo optical imaging of human retinal capillary networks using speckle variance optical coherence tomography with quantitative clinico-histological correlation. *Microvasc Res*. 2015;100:32–39.
63. Yu PK, Balaratnasingam C, Xu J, et al. Label-free density measurements of radial peripapillary capillaries in the human retina. *PLoS One*. 2015;10:e0135151.
64. Chui TY, Dubow M, Pinhas A, et al. Comparison of adaptive optics scanning light ophthalmoscopic fluorescein angiography and offset pinhole imaging. *Biomed Opt Express*. 2014;5: 1173–1189.
65. Kylstra JA, Brown JC, Jaffe GJ, et al. The importance of fluorescein angiography in planning laser treatment of diabetic macular edema. *Ophthalmology*. 1999;106:2068–2073.
66. Ffytche TJ, Shilling JS, Chisholm IH, Federman JL. Indications for fluorescein angiography in disease of the ocular fundus: a review. *J R Soc Med*. 1980;73:362–365.
67. Laatikainen L, Kohner EM. Fluorescein angiography and its prognostic significance in central retinal vein occlusion. *Br J Ophthalmol*. 1976;60:411–418.
68. Sjolie AK, Klein R, Porta M, et al. Retinal microaneurysm count predicts progression and regression of diabetic retinopathy: post-hoc results from the DIRECT Programme. *Diabet Med*. 2011;28:345–351.
69. Nunes S, Pires I, Rosa A, Duarte L, Bernardes R, Cunha-Vaz J. Microaneurysm turnover is a biomarker for diabetic retinopathy progression to clinically significant macular edema: findings for type 2 diabetics with nonproliferative retinopathy. *Ophthalmologica*. 2009;223:292–297.
70. Kohner EM, Stratton IM, Aldington SJ, Turner RC, Matthews DR. Microaneurysms in the development of diabetic retinopathy (UKPDS 42): UK Prospective Diabetes Study Group. *Diabetologia*. 1999;42:1107–1112.
71. Klein R, Meuer SM, Moss SE, Klein BE. Retinal microaneurysm counts and 10-year progression of diabetic retinopathy. *Arch Ophthalmol*. 1995;113:1386–1391.
72. Wise G. Retinal microaneurysms. *Arch Ophthalmol*. 1957; 151–156.
73. Cunha-Vaz JG. The blood-retinal barriers system: basic concepts and clinical evaluation. *Exp Eye Res*. 2004;78:715–721.
74. Guizar-Sicairos M, Thurman ST, Fienup JR. Efficient subpixel image registration algorithms. *Opt Lett*. 2008;33:156–158.

Investigative Ophthalmology & Visual Science